Atmos. Chem. Phys. Discuss., 9, 26199–26235, 2009
www.atmos-chem-phys-discuss.net/9/26199/2009/


Atmospheric Chemistry and Physics Discussions

This discussion paper is/has been under review for the journal Atmospheric Chemistry and Physics (ACP). Please refer to the corresponding final paper in ACP if available.

# The ground-based FTIR network's potential for investigating the atmospheric water cycle

**M. Schneider**[1], **K. Yoshimura**[2], **F. Hase**[1], **and T. Blumenstock**[1]

[1]Karlsruhe Institute of Technology (KIT), IMK-ASF, Karlsruhe, Germany
[2]Scripps Institution of Oceanography, University of California, San Diego, USA

Received: 26 November 2009 – Accepted: 27 November 2009 – Published: 9 December 2009

Correspondence to: M. Schneider (matthias.schneider@kit.edu)

Published by Copernicus Publications on behalf of the European Geosciences Union.





## Abstract

We present tropospheric $H_2^{16}O$ and $HD^{16}O/H_2^{16}O$ vapour profiles measured by ground-based FTIR (Fourier Transform Infrared) spectrometers between 1996 and 2008 at a northern hemispheric subarctic and subtropical site (Kiruna, Northern Sweden, 68° N and Izaña, Tenerife Island, 28° N, respectively). We compare these measurements to an isotope incorporated atmospheric general circulation model (AGCM). If the model is nudged towards meteorological fields of reanalyses data the agreement is very satisfactory on time scales ranging from daily to inter-annual which demonstrates the good quality of the FTIR data. Taking the Izaña and Kiruna measurements as an example we document the FTIR network's unique potential for investigating the atmospheric water cycle. For the subtropical site the FTIR observations confirm the central role of the Hadley circulation, but in addition they reveal a strong connection between the Northern Atlantic Oscillation (NAO) and the middle/upper tropospheric water vapour transport pathways. Concerning the subarctic site the observations indicate that water transport to the lower troposphere is affected by the northern Atlantic sea surface temperature and correlated to the Arctic Oscillation (AO). For the middle troposphere we observe that spring and autumn water transport pathways are different. We document in detail where the AGCM is able to capture these complexities of the water cycle and where it fails.

## 1 Introduction

For understanding and predicting climate change it is necessary to understand the whole complexity of the Earth's climate system wherein the atmospheric water cycle plays a central role. Water participates in many processes that are crucial for the Earth's climate. By distribution of heat (vertically and horizontally), regulating surface temperature, formation of clouds, radiative forcing due to water vapour, etc., it widely determines the energy budget and thus the climate of our planet. Improving the climate



ACPD

9, 26199–26235, 2009



models' treatment of the complex water cycle is one of the key goals set by the Intergovernmental Panel on Climate Change. In this context atmospheric water isotopologue ratios (e.g. $HD^{16}O/H_2^{16}O$) are of great interest. Various processes leave their imprint on the ratios: they are different, for instance, if evaporation happens from cold or warm ocean waters (and under dry or humid ambient conditions), from falling rain drops, from plants, or from the Earth's surface. Another example is recondensation while a humid air parcel moves to colder (higher) parts of the atmosphere. Then the vapour's depletion in heavy isotopologues (e.g. $HD^{16}O$) decreases gradually, generally the more pronounced the colder the temperatures. The isotopologue ratios of water contain valuable information about the history of the water mass and are thus a powerful tool for investigating the water cycle. In the following we express $H_2^{16}O$ and $HD^{16}O$ as $H_2O$ and HDO, respectively, and $HD^{16}O/H_2^{16}O$ as $\delta D = 1000‰ \times (\frac{[HD^{16}O]/[H_2^{16}O]}{SMOW} - 1)$, whereby $SMOW = 3.1152 \times 10^{-4}$ (SMOW: Standard Mean Ocean Water, Craig, 1961).

Incorporating isotopologues in atmospheric general circulation models (AGCMs) can provide unique opportunities to test and thereby improve the models' capability for reproducing the water cycle. By now global long-term tropospheric isotopologue simulations are available for several different AGCMs (for an overview see Sturm et al., 2009), but so far this promising research field remains widely unexplored due to the lack of comprehensive long-term high quality observational data (the measurements have to be very precise due to the small natural variability of the ratios). Until very recently precise measurements of tropospheric upper-air isotopologue ratios have been limited to sporadic campaigns (Ehhalt, 1974; Zahn, 2001; Webster and Heymsfield, 2003). Remote sensing techniques have the potential to provide quasi-continuous upper-air isotopologue ratio data. The sensors TES (Tropospheric Emission Spectrometer) and SCIAMACHY (Scanning Imaging Absorption Spectrometer for Atmospheric Chartography) have provided the first quasi-continuous observation of tropospheric $\delta$D, although for limited altitude ranges and time periods of a few years only (Worden et al., 2006; Frankenberg et al., 2009). In Schneider et al. (2006b) it is demonstrated that high quality ground-based FTIR (Fourier Transform Infrared) spectrometer measurements can



ACPD
9, 26199–26235, 2009



be used to retrieve $\delta$D between the surface and the middle/upper troposphere. These measurements have been performed since up to two decades at globally distributed sites within the NDACC (Network for Detection of Atmospheric Composition Change, Kurylo, 2000). The NDACC FTIR measurement records allow the generation of an unprecedented long-term dataset of tropospheric $\delta$D profiles.

In this paper we report tropospheric $H_2O$ and $\delta$D profiles measured by ground-based FTIR systems during up to 13 years at two very distinct sites: at the subarctic site of Kiruna and at the subtropical site of Izaña. We compare these measurements to the isotopologue incorporated AGCM, IsoGSM (Yoshimura et al., 2008). Section 2 briefly describes the measurement technique and the model. Section 3 presents the dataset, documents the difficulties faced when comparing observations and model, and the efforts taken to overcome these difficulties. Both sections can be skipped by a reader only interested in the scientific outcome of our study, which is presented in Sect. 4. There we present annual cycles, anomalies on different time scales, and connections to large scale anomalies of SST and atmospheric circulation. We reveal the unique potential of the FTIR technique for investigating the complexity of the atmospheric water cycle and document IsoGSM's capability of representing these complexities. Section 5 resumes the main results of our study.

## 2 Measurement and model techniques

### 2.1 The ground-based FTIR measurement technique

There are about 25 ground-based FTIR experiments performed within NDACC, among which the Kiruna and Izaña experiments. A ground-based FTIR system measures solar absorption spectra applying a high resolution Fourier Transform Spectrometer. The high resolution spectra allow an observation of the pressure broadening effect, and thus, the retrieval of trace gas profiles. The inversion problems faced in atmospheric remote sensing are in general ill-determined and the solution has to be





properly constrained. An extensive treatment of this topic is given in the textbook of C. D. Rodgers (Rodgers, 2000).

The retrieval of tropospheric water vapour amounts from measured ground-based FTIR spectra is a particularly demanding atmospheric inversion problem and, due to its large vertical gradient and variability, standard retrieval setups are not suited. The water vapour analysis applied for our study has been developed during the last years (Schneider and Hase, 2009) and has been extensively validated (Schneider et al., 2009). It works with the water vapour mixing ratios on a logarithmic scale and constrains the HDO and $H_2O$ ratios against each other, which is essential for an optimal estimation of tropospheric $H_2O$ and $\delta$D profiles (Schneider et al., 2006a,b). The $H_2O$ and $\delta$D profiles presented in the following are generated by analysing $H_2O$ and HDO signatures of the 1100–1330 $cm^{-1}$ wavenumber range.

### 2.2 The isotope-incorporated atmospheric general circulation model IsoGSM

IsoGSM is an isotope incorporated AGCM based on an up-to-date version of the Scripps Experimental Climate Prediction Centre's Global Spectral Model (ECPC's GSM; Kanamitsu et al., 2002). IsoGSM allows for nudging towards reanalysis large scale horizontal wind and temperature fields (Yoshimura and Kanamitsu, 2008). This technique assures that the model's atmospheric dynamics is in reasonable agreement with the real atmospheric dynamics. The horizontal resolution of the model is T62 (about 200 km) and the vertical resolution is 28 sigma-level layers. The output is in 17 pressure-level grid points, i.e. 1000, 925, 850, 700, 600, 500, 400, 300, 250, 200, 150, 100, 70, 50, 30, 20, and 10 hPa. For more details please refer to Yoshimura et al. (2008). IsoGSM data from a nudged run as well as from a free run (nudging turned off) are available on a global scale since 1979 with a temporal resolution of 6 h (red crosses in Figs. 1 and 2).



ACPD
9, 26199–26235, 2009



## 3 Presentation of the dataset

### 3.1 Subarctic site of Kiruna

Figure 1 shows the time series of measured and simulated $H_2O$ and $\delta$D data for the subarctic NDACC site of Kiruna (Northern Sweden, 67°50′ N, 20°25′ E at 420 m a.s.l.; e.g. Blumenstock et al., 2006). The ground-based FTIR measurements have been performed since March 1996 on a regular basis applying a Bruker IFS 120HR spectrometer. Typically there are about 80 measurement days per year. The gaps in the years 1999, 2000, 2004, and 2008 are due to the extremely stringent measurement quality that has to be required for isotopologue analysis. In the corresponding spectra we detect a small baseline offset (of about 1%, derived by analysing saturated water vapour signatures). It will be corrected in a future reevaluation and the data gaps for the corresponding years will be removed.

We present the total precipitable water vapour (PWV) amounts and the column integrated $\delta$D values, as well as the $H_2O$ volume mixing ratios (VMRs) and $\delta$D values for the lower free troposphere, and the middle troposphere, represented by the altitudes of 1 and 4 km, respectively. Concerning $H_2O$ we observe a very prominent annual cycle in both measurements and simulations. There are some small systematic differences: close to the surface the modeled water vapour amounts are slightly lower than the measured amounts and in the middle troposphere the modeled amounts are slightly larger than the measured amounts. Concerning $\delta$D we observe more variability in the measurement as compared to the model. In the middle troposphere (4 km) there is a large systematic difference. Whereas the $\delta$D values simulated for 4 km are confined between −200 and −500‰, the measured values are situated between ± 0‰ in summer and −400‰ in winter.



ACPD
9, 26199–26235, 2009



### 3.2 Subtropical site of Izaña

The time series of simulation and measurements for the NDACC site of Izaña (Tenerife Island, Spain, 28°18′ N, 16°29′ W at 2370 m a.s.l.; e.g. Schneider et al., 2008) are depicted in Fig. 2. We show $H_2O$ and $\delta$D data for altitudes of 3 and 7 km, which are representative for the lower free and the middle subtropical troposphere and for the column integrated atmosphere. The FTIR measurements started in March 1999 applying a Bruker IFS 120M spectrometer. In January 2005 the IFS 120M was replaced by a Bruker IFS 120/5HR spectrometer. As for Kiruna we apply a very stringent measurement quality criterion. The FTIR $\delta$D profile data are limited to 4 years, since the IFS 120M measurements, performed in the 1000–1330 $cm^{-1}$ range do generally not reach the high signal to noise ratio that is required for measuring $\delta$D profiles. In the near future we hope to close these gaps by an additional analysis of $H_2O$ and HDO signatures in the 2600–3100 $cm^{-1}$ wavenumber range, where the signal to noise ratio is significantly higher.

The annual $H_2O$ cycles are less pronounced than in Kiruna. Concerning the PWV amounts measurements and simulations agree very well. Similar to Kiruna we observe a slight dry bias of the model with respect to the measurement in the lower troposphere and a wet bias in the middle troposphere. Both measurement and simulation observe a maximum in $\delta$D in summer and a minimum in winter. However, similar to Kiruna, the amplitude of the cycle is larger for the measurements if compared to the simulations. Furthermore there is a systematic difference between the middle tropospheric $\delta$D values: whereas the typically measured $\delta$D value is −210‰, the typically simulated value is −260‰.

### 3.3 Disparity between FTIR and IsoGSM data

When comparing model and remote sensing data it is important to think about disparities between the data. Both model and remote sensing data have different characteristics, which have to be considered when interpreting differences of the measured



ACPD
9, 26199–26235, 2009



and modeled data. Here we discuss the differences between IsoGSM and FTIR with respect to vertical resolution, horizontal resolution, temporal resolution, and sampling frequency.

1. Vertical resolution: The vertical resolution of the FTIR $H_2O$ and $\delta$D profiles is indicated by the averaging kernels shown in Fig. 3 for typical Kiruna and Izaña measurements. Concerning $H_2O$ and defined as full width half maximum of the averaging kernels, the vertical resolution is 2 km in the lower troposphere, 4 km in the middle troposphere, and 6 km in the upper troposphere. The vertical resolution of the $\delta$D profiles is coarser: about 3 km in the lower troposphere and 6 km in the middle troposphere. Typical degree of freedoms are 2.6 for $H_2O$ and 1.6 for $\delta$D. Figure 3 also depicts the sum of all averaging kernels (thick solid black line), which indicates the total sensitivity of the FTIR system with respect to $H_2O$ and $\delta$D. For Kiruna the FTIR system is well sensitive up to an altitude of 7 km (more than 75% of the atmospheric $H_2O$ and $\delta$D variability is detected by FTIR, see curve $\Sigma_{row}$). For Izaña these sensitivity range is extended up to 10–11 km. In contrast to the coarse vertical resolution of the FTIR profiles the model resolves much more vertical details. For the following analyses we smooth the modeled profiles with the FTIR averaging kernels. Thereby we assures that measured and simulated profiles represent the same details of the vertical $H_2O$ and $\delta$D structures.

2. Horizontal resolution: The FTIR data represent the atmosphere along the straight line that connects the sun and the ground-based FTIR spectrometer. It is near to a punctiform measurement. On the other hand, the vertical resolution of the model is 200 km and consequently the model data represent the atmosphere as averaged over a 200×200 km area. From this point of view we expect that the FTIR data show more short-term variability than the model data. This disparity increases the scatter between measurements and simulations but averages out when contemplating long time scales.



ACPD
9, 26199–26235, 2009



3. Temporal resolution: The temporal extent of the FTIR measurements is in the order of minutes. The measurements are well able to detect instantaneous small scale features. On the contrary, the model's temporal output step is 6 h (although its time step is less than 30 min). It represents atmospheric features averaged over 6 h. This disparity will cause the FTIR data to be more variable on short time scales than the model data. As for the horizontal resolution, this disparity averages out when contemplating longer time scales.

4. Sampling frequency: The FTIR measurements are only performed for clear sky conditions and only represent the atmosphere for a short instant. On the other hand the model provides continuous data. It is representative for all atmospheric conditions. In the following we only apply model data that temporarily match with the FTIR data within 3 h, which reduces the effects of this disparity.

### 3.4 Statistics on the IsoGSM-FTIR differences

In Fig. 4 we show a statistics of the comparison between daily mean values of FTIR measurements and coincident IsoGSM simulations smoothed by the FTIR averaging kernels. These statistics are based on coincidences for about 770 and 400 different days for Kiruna and Izaña, respectively. The lower panels show the mean difference and the $1\sigma$ scatter of the difference of the $H_2O$ VMRs. The characteristic of the model-measurement difference is very similar for Kiruna and Izaña. In the lower troposphere the model underestimates and in the middle/upper troposphere the model overestimates the measured $H_2O$ VMRs. These observations are in line with the study of John and Soden (2007) who report a systematic boundary layer dry bias and a free tropospheric wet bias for a variety of different AGCMs. As grey line and area in the lower right panel we depict the statistics of the difference between Vaisala RS92 radiosonde and FTIR measurements performed simultaneously between 2005 and 2008 at Izaña (Schneider et al., 2009). It documents the good quality of the FTIR $H_2O$ profiles.



ACPD
9, 26199–26235, 2009



The top panels of Fig. 4 depict the mean difference and 1$\sigma$ scatter between measured and simulated $\delta$D profiles. For both sites we observe a systematic difference between the IsoGSM and FTIR middle/upper tropospheric $\delta$D of about 100‰. This difference is larger for Kiruna as compared to Izaña. In both cases we already observe a systematic difference between FTIR and $\delta$D climatologies, which are constructed from a variety of different in-situ measurements (Taylor , 1972; Ehhalt, 1974; Zahn, 2001) and applied as a priori $\delta$D profiles for the FTIR retrieval. The mean differences of the FTIR $\delta$D profiles and the in-situ profiles are depicted as grey dashed line in the top panels of Fig. 4. The FTIR systematically underestimates the tropospheric HDO depletion measured by the in-situ experiments. However, the in-situ data are collected at sites and times that differ from the FTIR measurements and consequently this comparison is subject to large uncertainties. On the other hand already an error of only 5% in the spectroscopic pressure broadening coefficients applied in the FTIR retrieval could cause a systematic error of 100‰. We think that most of the systematic difference between the FTIR and in-situ profiles is due to a bias in the FTIR data.

The scatter between the FTIR and IsoGSM $\delta$D is about 50‰ for the lower troposphere in Kiruna and about 80‰ for the middle troposphere in Kiruna and for the lower and middle troposphere in Izaña. This is more than what we estimated for the FTIR $\delta$D precision, which is 15‰ for the lower troposphere and 40‰ for the middle troposphere (Schneider et al., 2006b). The magnitude of the observed scatter cannot be explained by uncertainties in the FTIR data. It must be due to disparities between the FTIR and IsoGSM data (see Sect. 3.3) and/or due to differences between the real atmosphere and the IsoGSM simulations.

## 4 Scientific interpretation of the time series

In this section we perform a detailed analysis of the the measured time series and modeled time series for both, nudged- and free-run IsoGSM simulations. Nudging towards the reanalysis data assures that the dynamics produced by the model is in



ACPD
9, 26199–26235, 2009



satisfactory agreement with the real atmospheric dynamics. The free-run simulations are only driven by SST temperature, which is how common AMIP-type (Atmospheric Model Intercomparison Project; Gates, 1992) AGCMs operate.

### 4.1 The method

Figures 1 and 2 show that the annual cycles are the dominating signatures in the tropospheric $H_2O$ and $\delta$D time series. The annual cycles are superimposed by short time scale variability and possible inter-annual variability. The objective of the data analysis method is to compare measurement and model on different time scales and to identify the different underlying processes for the variability. Therefore, we construct a function $F$, that consists of several parameter functions that we assume to be the major variability sources:

$$\begin{aligned} F = & f_0 + f_1 \cos 2\pi t + f_2 \sin 2\pi t \\ & + f_3 \cos 4\pi t + f_4 \sin 4\pi t \\ & + f_5 \cos 6\pi t + f_6 \sin 6\pi t \\ & + f_l(t) \\ & + f_{\text{sens}}(t) \\ & + f_C(\overline{\ln[\mathrm{H_2O}]} - \ln[\mathrm{H_2O}](t)) \end{aligned} \quad (1)$$

The different parameter functions are then fitted simultaneously – in a least squares sense – to the measured and modeled time series. By a bootstrap method (e.g. Gardiner et al., 2008) we can estimate the significance of the correlations between the different parameter functions and the dataset.

The first three lines on the right hand side of Eq. (1) account for the annual cycle, which is modeled in terms of a Fourier series where $t$ is measured in years, and $f_0$ to $f_6$ are the parameters of the Fourier series. We consider frequencies up to 3 year$^{-1}$. This turns out to be sufficient and yields to very robust fitting results.



ACPD
9, 26199–26235, 2009



The fourth line of Eq. (1), $f_I(t)$, contains the time series of climatological indices, that are assumed to affect the transport of water through the atmosphere. In order to get stable fitting results the applied indices must be uncorrelated. For each site we fit two different indices: a first index describing patterns of atmospheric circulation variability (the Arctic Oscillation (AO) index for Kiruna and the Northern Atlantic Oscillation (NAO) index for Izaña), and a second index describing SST anomalies (the Atlantic Multi-decadal Oscillation (AMO) index for Kiruna and the Tropical Northern Atlantic (TNA) index for Izaña).

The fifth line of Eq. (1), $f_{\text{sens}}(t)$, accounts for the variation of the FTIR system's sensitivity. It contains a time series of the altitude specific sensitivity value (thick black line, $\Sigma_{\text{row}}$, of Fig. 3). The simultaneous fit of $f_{\text{sens}}(t)$ reduces the impact of systematic errors (e.g. due to spectroscopic parameters) on the data analysis.

The sixth line of Eq. (1) accounts for the correlation between $H_2O$ and $\delta$D. Assuming Rayleigh distillation, changes of water vapour amounts ($d\ln[H_2O]$) and changes of $\delta$D in the vapour phase (represented by $d\ln\frac{[HDO]}{[H_2O]}$) are connected via the following relation (e.g. Dessler and Sherwood, 2003):

$$(\alpha - 1) d\ln[H_2O] = d\ln\frac{[HDO]}{[H_2O]} \tag{2}$$

whereby $\alpha$ is the equilibrium fractionation coefficient (van Hook , 1968). Since $\alpha$ depends on temperature and since Rayleigh distillation is only one of several different fractionation processes, the relation between $\ln[H_2O]$ and $\ln\frac{[HDO]}{[H_2O]}$ depends on the history of the analysed airmass and varies from day to day. Nevertheless, there is a strong correlation between $\ln[H_2O]$ and $\ln\frac{[HDO]}{[H_2O]}$ concerning both the model and the measurement (see Fig. 5). The slope of the corresponding regression lines ($\overline{\alpha} - 1$) is a measure for the typical water transport pathways. We estimate ($\overline{\alpha} - 1$) by fitting a function $f_C$ to the $\delta$D time series. The function $f_C$ describes by how much the actual logarithm of the $H_2O$ amount ($\ln[H_2O](t)$) deviates from its mean value ($\overline{\ln[H_2O]}$). Therein, we



ACPD
9, 26199–26235, 2009



have to consider that the FTIR system can observe much finer $H_2O$ than $\delta$D structures (see Fig. 3) and construct a function $f_C$ applying $H_2O$ data smoothed by the $\delta$D averaging kernels.

As described by Eq. (1) we fit 10 different parameter function to the $H_2O$ time series and 11 (when including $f_C$) different parameter functions to the $\delta$D time series. In the case of Kiruna the time series consist of 1700 individual FTIR observations made on 770 different days between 1996 and 2008. At Izaña so far only the IFS 120/5HR data fulfill the stringent quality criterion required for $\delta$D profile observations. In this case we analyse the time series between 2005 and 2008 only. It consists of more than 850 individual FTIR observations made on 400 different days.

### 4.2 Correlations between $H_2O$ and $\delta$D

In this subsection we estimate the importance of the term $f_C$ of Eq. (1) for the $\delta$D time series. Figure 6 depicts the slopes $(\overline{\alpha}-1)$ determined by our multi-regression method throughout the troposphere. Black, red, and green curves represent the results from the measurements, the nudged model run, and the free model run, respectively. The hatched area around the curves indicate the $1\sigma$ (i.e. 67%) significance area. The slope $(\overline{\alpha}-1)$ contains information about the mean situation (typically involved pathways and fractionation processes). At both sites $(\overline{\alpha}-1)$ as derived from the measurement decreases with height, whereas for the models it tends to increase with height.

The significant differences of $(\overline{\alpha}-1)$ between measurement and model indicate a systematic error in the model. The error is not reduced by nudging the model towards the dynamic fields of reanalyses data, which allows excluding large scale transport processes as an error source. Instead the known deficits of AGCMs in reproducing large scale humidity fields (John and Soden, 2007) might be the reason. Furthermore, an incorrect parameterisation of small scale processes, like sub-scale mixing, inner-cloud processes, fractionation processes, etc., might play a role. Here we only document these deficits and advert that identifying and removing them is very important for further progress in applying isotopologue models for climate change research.



ACPD
9, 26199–26235, 2009



In the following we analyse all $\delta$D time series twice by two different fits to the model function $F$ of Eq. (1): a first without the term $f_C$ and a second with the term $f_C$ included. We call the $\delta$D values resulting from an analysis with the term $f_C$ included $\delta$D' values. By producing the $\delta$D' values we partly remove the aforementioned model deficits, although we do not know their exact reason. Furthermore, the $\delta$D' values are independent from the $H_2O$ values and thus reveal the actual gain of information by measuring HDO in addition to $H_2O$.

### 4.3 Annual cycles

Figure 7 depicts the annual cycles as derived for Kiruna by fitting function $F$ to the dataset. There is a good agreement between the annual evolution of modeled (red line for nudged run, green line for free run) and measured (black line) $H_2O$. Model and measurement indicate a pronounced $H_2O$ maximum in July/August for PWV, the lower, and the middle troposphere. As already shown in Fig. 4, the modeled middle tropospheric water vapour amounts are systematically larger than the measured amounts (due to the aforementioned wet bias in AGCMs; e.g. John and Soden, 2007).

Concerning column integrated and lower tropospheric $\delta$D both model and measurements reproduce the maximum in summer, but the amplitude (peak to peak difference between summer and winter) is larger in the measured than in the modeled cycle. These amplitudes are slightly reduced from $\delta$D' indicating indicating that the water vapour transport pathways to Kiruna's lower troposphere are during the whole year very similar: the water vapour evaporates in the Atlantic Ocean and is transported efficiently to Northern Scandinavia. The situation changes completely in the middle troposphere where the differences between modeled and measured $\delta$D are very large. While the FTIR observes a $\delta$D maximum in April/May and enhanced values until October, the IsoGSM maximum is confined within July and August in parallel to the $H_2O$ maximum. The large amplitude in the measured $\delta$D' cycle suggests large intra-annual variability in the water vapour transport pathways to Kiruna's middle troposphere and/or large intra-annual variability in the involved fractionation processes. Between spring



ACPD
9, 26199–26235, 2009



(high $\delta$D' values) and autumn (low $\delta$D' values) the transport processes and/or involved fractionation processes differ systematically. This suggests different water source region for spring and autumn, a situation that is not captured by the model.

The annual cycles for Izaña are shown in Fig. 8. The agreement between nudged run model (red line) and measurement (black line) is similar to Kiruna: $H_2O$ cycles agree well throughout the troposphere (besides the model's middle/upper tropospheric wet bias). Concerning $\delta$D, the agreement is satisfactory but with a slightly larger amplitude in the measured than in the modeled cycle. This difference in the amplitude is widely eliminated for $\delta$D'. It is very interesting that model and measurement reveal two maxima: a first one in March/April and a second one in August. This August maxima is a surprise since the Hadley cell is intense over the northern hemispheric subtropics until the end of October and correspondingly a minimum in $\delta$D and $\delta$D' should be expected throughout the summer. However at Izaña, due to its location close to the African west coast, we have to deal with a particular feature: the combination of the African mid-tropospheric high, centered typically in South Western Algeria at 25° N and of the African Easterly Jet, which develops in Northern Hemispheric summer at 15° N between 30° W and 20° E, favours the transport of humid lower tropospheric air into the Canarian middle troposphere (Cook, 1999; Chen, 2006). The free run model (green line) is not able to capture this regional feature. It simulates summer troposphere dominated by the Hadley circulation with middle/upper tropospheric $H_2O$, $\delta$D, and $\delta$D' values being relatively low during the entire summer.

As a detail we observe a small time shift of about 1–2 months in the the August/September maxima between nudged run model and measurement. This might be due to a small scale local feature, that cannot be captured by the model: continuous heating of the Island of Tenerife during summer may induce small scale circulations above the Island. This circulation is most pronounced at the end of summer and transports very effectively low tropospheric humid air to higher altitudes.



ACPD
9, 26199–26235, 2009



### 4.4 Short-term variability and anomalies

In this subsection we compare measured and modeled data after removing the annual cycle, i.e. we contemplate deseasonalised data. This allows a validation of the model on different time scales independent from the systematic model-measurement differences presented in Figs. 7 and 8.

Figure 9 shows profiles of the coefficient of determination ($R^2$) for deseasonalised daily mean and quarterly mean variability. In the case of a linear correlation $R^2$ is the portion of the variance of the measured data that can be explained by the modeled data. An $R^2$ of 1 means that the model explains all the variance in the measured $H_2O$ or $\delta$D data, and an $R^2$ of 0 means that model and measurement are completely uncorrelated. The red line and hatched area represent the $R^2$ values and the $1\sigma$ confidence interval for the nudged-run comparison and the green line and hatched area the results for the free-run comparison. Concerning the nudged-run data all correlation are significant at a 95% confidence level. In the lower troposphere the nudged model explains 70% of the measured $H_2O$ variances, and in the middle/upper troposphere still 50%. These values generally increase when averaging over longer time scales, since such averaging reduces the scatter that is introduced by differences in the horizontal and temporal resolution between model and measurements (see discussion of Sect. 3.3). Averaging is especially important for the free run data. For short time scales there is nearly no probability for a correlation between measurement and model, whereby for the quarterly mean data there is a significant probability for a moderate correlation between the FTIR data and the free run model data. For $\delta$D the coefficients $R^2$ are slightly lower than for $H_2O$. Concerning the nudged model and the lower troposphere we achieve a value of 50% for daily mean data and of 60% quarterly mean data. At higher altitudes the correlation is rather week. For $\delta$D' the correlation is significantly stronger than for $\delta$D, since $\delta$D' accounts for some of the deficits in the model (see discussion in Subsect. 4.2). Then we get a lower tropospheric $R^2$ of more than 70% on a daily time scale and 90% on a quarterly time scale. These strong correlations



ACPD
9, 26199–26235, 2009



document that in the lower troposphere the model – apart form the deficits as discussed in Subsect. 4.2 – performs very well and that the FTIR data are of very good quality. The correlation with free run $\delta$D' data is also good.

Figure 10 informs about the performance of the model in the subtropical atmosphere of Izaña. Generally the correlations are poorer if compared to Kiruna (e.g. at Izaña $R^2$ values for daily mean data are all below 30%, whereas at Kiruna 75% are achieved). Correlating Izaña's FTIR $H_2O$ amounts with corresponding Vaisala RS92 radiosonde amounts yield $R^2$ values of about 95%, which demonstrates that the relatively poor FTIR-IsoGSM correlations at Izaña are due to incorrect model data. While at Kiruna the situation is rather uniform during the whole year, the Izaña atmosphere is affected by two very distinct atmospheric patterns, the Hadley circulation, which prevails in summer, and the westerlies, which are important in winter. It seems that the model has problems to capture the implicated temporal and spatial inhomogeneities. Furthermore, the Izaña measurements represent exclusively altitudes above 2.4 km, where AGCM humidity simulations are known to be particularly strong wet-biased.

### 4.5 Large-scale climate patterns

In this subsection we investigate if the anomalies of the $H_2O$ and $\delta$D profiles – represented by the deseasonalised quarterly mean data analysed in Figs. 9 and 10 – are connected to atmospheric and oceanic large scale patterns. Therefore, we study the importance of function $f_I$ of Eq. (1). For Kiruna we construct a function $f_I$ which contains the indices of the Arctic Oscillation (AO) and of the Atlantic Oscillation Multidecadal (AMO). The AO index describes 1000 mb height anomalies north of 20° N. It represents large scale atmospheric anomalies of the Northern Hemisphere. The AMO index is calculated from Atlantic SST anomalies north of the Equator and is representative for the oceanic anomalies in the northern Atlantic. Figure 11 shows the coefficient of determination $R^2$ (multiplied with the sign of the slope of the linear regression line)



ACPD
9, 26199–26235, 2009



for the correlation between measured and modeled $H_2O$, $\delta$D, and $\delta$D' profiles and the AO and AMO indices at Kiruna. We find that both $H_2O$ and $\delta$D is positively correlated with the AO index (see left panels). The correlation is in particulary strong for the lower troposphere, where about 30% of the measured (black curves) and nudged model run anomalies (red curves) in $H_2O$ and $\delta$D can be explained by the AO index. The hatched area in the panels represent the $1\sigma$ (66%) significance intervals and demonstrate that the correlations are highly significant. The green curves show the situation for the free model run. In this case we also observe some correlation for lower tropospheric $H_2O$ and $\delta$D, however, the slope of the linear regression line has the opposite sign if compared to the FTIR measurements and the nudged run simulations: the free run model is not able to correctly capture the importance of the Arctic Oscillation for Kiruna's lower tropospheric water vapour. For $\delta$D' the correlations is still strong, which means that the AO index is mainly correlated with atypical water vapour transport pathways. The model as well as the measurement clearly reveal a connection between the AO index and the water transport pathways to Kiruna's lower troposphere.

The right panels of Fig. 11 depict the correlations with the AMO index. The most significant correlation is found for $\delta$D' in the lower troposphere, where about 20% of the measured and nudged run $\delta$D' anomalies can be explained by Atlantic SST anomalies. This correlations are significant on a 95% significance level, and reveal a climate feedback: increased surface temperatures will increase SST, which will apparently lead to changes in Kiruna's lower tropospheric water vapour transport pathways. The free run model shows no correlations.

Figure 12 demonstrates that a consistent long-term dataset is mandatory for identifying the above described connections. It shows correlation plots between the Arctic Oscillation Index and the $\delta$D anomalies as measured at Kiruna at an altitude of 1 km for different time scales (short-term, monthly, quarterly, and yearly). On short time scales there is a large scatter in the $\delta$D data due to the large day-to-day variability. Then we cannot observe a clear connection between Kiruna's lower tropospheric $\delta$D and the AO index ($R^2$ of only 6.3%). This connection gets only significant when averaging over



ACPD
9, 26199–26235, 2009



longer time scales. When contemplating quarterly mean data the $R^2$ value is almost 40%.

Figure 13 shows the correlation between the Izaña data and the Northern Atlantic Oscillation (NAO) index (left panels) and the Tropical Northern Atlantic (TNA) index (right panels). The NAO index describes northern hemispheric anomalies of the 500 mb height. It represents large scale atmospheric anomalies. The TNA index is constructed from SST anomalies in the Tropical Atlantic between 5° N and 25° N. We find a very strong and significant negative correlation between the the NAO index and the measured middle/upper tropospheric $\delta$D and $\delta$D' (at a 99% confidence level). The corresponding correlations with the nudged model data are weaker and not very significant. The measurements clearly suggest that the atmospheric anomalies described by the NAO index affect the water transport to Izaña's middle/upper troposphere. This is a very exciting result and manifests the large complexity of the water cycle in the subtropics. The model fails in capturing the complexity of the subtropics, which is of great importance on a global scale, since the tropical dry zone is the key region of the water vapour feedback effect (Pierrehumbert, 1995; Spencer and Braswell, 1997; Held and Soden, 2000). Climate projection based on models that are not able to reproduce this important aspect of the Earth's climate system should be treated with great care.

The right panels of Fig. 13 show the correlations to the tropical northern Atlantic SST anomalies (as described by the TNA index). There is a very strong and significant correlation between the measured middle/upper tropospheric $H_2O$ amounts and the TNA index. About 60% of the measured $H_2O$ anomalies can be explained by anomalies in the SST of the tropical northern Atlantic A significant positive correlation is also seen between the TNA index and the measured middle/upper tropospheric $\delta$D Tropical SST is well positively correlated with tropical upper tropospheric specific humidity (e.g. Minschwaner et al., 2006). Our observation of a strong correlation between tropical SST and the subtropical middle troposphere is a consequence of the direct connection between the tropical upper troposphere and the subtropical middle troposphere by means of the Hadley circulation. The nudged model does not well capture the strength



ACPD
9, 26199–26235, 2009



of the correlation between TNA and subtropical middle tropospheric $H_2O$ (red curve in the bottom right panel), which might indicates that it underestimates the effectiveness of the connection between tropical upper troposphere and subtropical middle troposphere.

## 5 Conclusions

The long-term comparison of FTIR measurements and IsoGSM simulations confirms the high quality of the FTIR $H_2O$ and $\delta$D data estimated in previous studies (Schneider et al., 2006b; Schneider and Hase, 2009, and references therein). Currently the ground-based FTIR technique is the only technique that can provide tropospheric profiles of $H_2O$ and $\delta$D at a satisfactory and well-documented precision and over the long time periods required for extensive studies of the atmospheric water cycle. The Kiruna FTIR data reveal a strong connection between lower tropospheric water transport pathways and the AO index. At the same time they suggest that these transport pathways will change in response to global warming (correlation between $\delta$D' and AMO index). Furthermore, they reveal systematic spring to autumn differences concerning the processes that determine middle/upper tropospheric water amounts. For the subtropical site of Izaña the FTIR data document the importance of the Hadley circulation and a surprisingly strong correlation between middle/upper tropospheric water vapour transport pathways and the NAO index.

It is very exiting that the Kiruna and Izaña FTIR measurements, in representation of the entire ground-based FTIR network, are able to identify these climate feedback mechanisms and complexities of the water cycle, since they are responsible for the main uncertainties in current climate models. The FTIR data open up new opportunities for improving climate models by means of isotopologues and our study is pioneering in this promising and innovative research field. We show that the quality of the $\delta$D simulations of the model IsoGSM strongly depends on the accuracy of the modeled dynamics. Only if the model is nudged towards the meteorological fields of reanalyses



ACPD
9, 26199–26235, 2009



data IsoGSM is able to capture the complexity of the subarctic atmospheric water cycle. Nudging is also important for simulating the atmospheric cycle in the subtropics, but even the nudged model fails in reproducing the strong connection between the middle/upper tropospheric water vapour transport and the NAO index. This is a severe deficit of a climate model since understanding the water cycle in the tropical dry zones is of ultimate importance for understanding Earth's climate. The known systematic biases when modelling hydrology fields and errors related to the parameterisation of small scale processes (both not nudged) are potential sources for these model deficits.

If not nudged towards reanalyses data and only driven by SST (AMIP-type model) the model is not able to reproduce the historical atmospheric patterns described by NAO and AO and consequently their connections to $H_2O$ and $\delta$D are not captured. Furthermore, then the responses of the atmospheric water cycle to SST are only partially reproduced. This is not very satisfactory since climate prediction models cannot be nudged. In a future study it should be investigated if fully coupled ocean-atmosphere models perform better in this respect.

*Acknowledgements.* M. Schneider is funded by the Deutsche Forschungsgemeinschaft (project RISOTO: Geschäftszeichen SCHN 1126/1-1 and 1-2). We are grateful to the Goddard Space Flight Center for providing the temperature and pressure profiles of the National Centers for Environmental Prediction via the automailer system and to U. Raffalski for assisting us with the FTIR experiment in Kiruna.

## References

Blumenstock, T., Kopp, G., Hase, F., Hochschild, G., Mikuteit, S., Raffalski, U., and Ruhnke, R.: Observation of unusual chlorine activation by ground-based infrared and microwave spectroscopy in the late Arctic winter 2000/01, Atmos. Chem. Phys., 6, 897–905, 2006, http://www.atmos-chem-phys.net/6/897/2006/. 26204

Chen, T.-C.: Characteristics of African Easterly Waves depicted by ECMWF Reanalysis for 1991–2000, Mon. Wea. Rev., 134, 3539–3566, 2006. 26213





Cook, K. H.: Generation of the African Easterly Jet and its role in determinating West African precipitation, J. Climate, 12, 1165–1184, 1999. 26213
Craig, H.: Standard for Reporting Concentrations of Deuterium and Oxygen-18 in Natural Waters, Science, 133, 1833–1834, doi:10.1126/science.133.3467.1833, 1961. 26201
Dessler, A. E. and Sherwood, S. C.: A model of HDO in the tropical tropopause layer, Atmos. Chem. Phys., 3, 2173–2181, 2003, http://www.atmos-chem-phys.net/3/2173/2003/. 26210
Ehhalt, D. H.: Vertical profiles of HTO, HDO, and $H_2O$ in the Troposphere, Rep. NCAR-TN/STR-100, Natl. Cent. for Atmos. Res., Boulder, Colo., 1974. 26201, 26208
Frankenberg, C., Yoshimura, K., Warneke, T., Aben, I., Butz, A., Deutscher, N., Griffith, D., Hase, F., Notholt, J., Schneider, M., Schrejver, H., and Röckmann, T.: Dynamic processes governing lower-tropospheric HDO/$H_2O$ ratios as observed from space and ground, Science, 325, 1374–1377, doi:10.1126/science.1173791, 2009. 26201
Gates, W. L.: AMIP: The Atmospheric Model Intercomparison Project, Bull. Am. Meteorol. Soc., 73, 1962–1970, 1992. 26209
Gardiner, T., Forbes, A., de Mazière, M., Vigouroux, C., Mahieu, E., Demoulin, P., Velazco, V., Notholt, J., Blumenstock, T., Hase, F., Kramer, I., Sussmann, R., Stremme, W., Mellqvist, J., Strandberg, A., Ellingsen, K., and Gauss, M.: Trend analysis of greenhouse gases over Europe measured by a network of ground-based remote FTIR instruments, Atmos. Chem. Phys., 8, 6719–6727, 2008, http://www.atmos-chem-phys.net/8/6719/2008/. 26209
Held, I. M. and Soden, B. J.: Water Vapour Feedback and Global Warming, Annu. Rev. Energy Environ., 25, 441–475, 2000. 26217
John, V. O. and Soden, B. J.: Temperature and humidity biases in global climate models and their impact on climate feedbacks, Geophys. Res. Lett., 34, L18704, doi:10.1029/2007GL030429, 2007. 26207, 26211, 26212
Kanamitsu, M., Kumar, A., Juang, H.-M. H., Schemm, J.-K., Wang, W., Yang, F., Hong, S.-Y., Peng, P., Chen, W., Moorthi, S., and Ji, M.: NCEP dynamical seasonal forcast system 2000, Bull. Am. Meteorol. Soc., 83, 1019–1037, 2002. 26203
Kurylo, M. J. and Zander, R.: The NDSC – Its status after 10 years of operation, Proceedings of XIX Quadrennial Ozone Symposium, Hokkaido University, Sapporo, Japan, 167–168, 2000. 26202
Minschwaner, K., Desler, A. E., and Sawaengphokhai, P.: Multimodel Analysis of the Water



ACPD
9, 26199–26235, 2009



Vapor Feedback in the Tropical Upper Troposphere, J. Climate, 19, 5455–5465, 2006. 26217
Pierrehumbert, R. T.: Thermostats, Radiator Fins, and the Local Runaway Greenhouse, J. Atmos. Sci., 52, 1784–1806, 1995. 26217
Rodgers, C. D.: Inverse Methods for Atmospheric Sounding: Theory and Praxis, World Scientific Publishing Co., Singapore, ISBN 981-02-2740-X, 2000. 26203
Schneider, M., Hase, F., and Blumenstock, T.: Water vapour profiles by ground-based FTIR spectroscopy: study for an optimised retrieval and its validation, Atmos. Chem. Phys., 6, 811–830, 2006, http://www.atmos-chem-phys.net/6/811/2006/. 26203
Schneider, M., Hase, F., and Blumenstock, T.: Ground-based remote sensing of HDO/$H_2O$ ratio profiles: introduction and validation of an innovative retrieval approach, Atmos. Chem. Phys., 6, 4705–4722, 2006, http://www.atmos-chem-phys.net/6/4705/2006/. 26201, 26203, 26208, 26218
Schneider, M., Redondas, A., Hase, F., Guirado, C., Blumenstock, T., and Cuevas, E.: Comparison of ground-based Brewer and FTIR total column $O_3$ monitoring techniques, Atmos. Chem. Phys., 8, 5535–5550, 2008, http://www.atmos-chem-phys.net/8/5535/2008/. 26205
Schneider, M. and Hase, F.: Ground-based FTIR water vapour profile analyses, Atmos. Meas. Tech., 2, 609–619, 2009, http://www.atmos-meas-tech.net/2/609/2009/. 26203, 26218
Schneider, M., Romero, P. M., Hase, F., Blumenstock, T., Cuevas, E., and Ramos, R.: Quality assessment of Izaña's upper-air water vapour measurement techniques: FTIR, Cimel, MFRSR, GPS, and Vaisala RS92, Atmos. Meas. Tech. Discuss., 2, 1625–1662, 2009, http://www.atmos-meas-tech-discuss.net/2/1625/2009/. 26203, 26207
Spencer, R. W. and Braswell, W. D.: How Dry is the Tropical Free Troposphere? Implications for Global Warming Theory, Bull. Amer. Meteor. Soc., 78, 1097–1106, 1997. 26217
Sturm, C., Zhang, Q., and Noone, D.: An introduction to stable water isotopes in climate models: benefits of forward proxy modelling for paleoclimatology, Clim. Past Discuss., 5, 1697–1729, 2009, http://www.clim-past-discuss.net/5/1697/2009/. 26201
Taylor, C. B.: The vertical variations of the isotopic concentrations of tropospheric water vapour over continental Europe and their relationship to tropospheric structure, N. Z. Dep. Sci. Ind. Res., Inst. Nucl. Sci. Rep., INS-R-107, 44 pp., 1972. 26208



ACPD
9, 26199–26235, 2009



van Hook, W. A.: Vapor pressures of the isotopic waters and ices, J. Phys. Chem., 72, 1234–1244, 1968. 26210

Webster, C. R. and Heymsfield A. J.: Water isotope ratios D/H, $^{18}O/^{16}O$, $^{17}O/^{16}O$ in and out of clouds map dehydration pathways, Science, 302, 1742–1745, 2003. 26201

Worden, J. R., Bowman, K., Noone, D., Beer, R., Clough, S., Eldering, A., Fisher, B., Goldman, A., Gunson, M., Herman, R., Kulawik, S. S., Lampel, M., Luo, M., Osterman, G., Rinsland, C., Rodgers, C., Sander, S., Shephard, M., and Worden, H.: TES observations of the tropospheric HDO/$H_2O$ ratio: retrieval approach and characterization, J. Geophys. Res., 111(D16), D16309, doi:10.1029/2005JD006606, 2006. 26201

Yoshimura, K., Kanamitsu, M., Noone, D., and Oki, T.: Historical isotope simulation using Reanalysis atmospheric data, J. Geophys. Res., 113, D19108, doi:10.1029/2008JD010074, 2008. 26202, 26203

Yoshimura, K. and Kanamitsu, M.: Dynamical global downscalling of global reanalysis, Mon. Wea. Rev., 136(8), 2983–2998, 2008. 26203

Zahn, A.: Constraints on 2-Way Transport across the Arctic Tropopause Based on $O_3$, Stratospheric Tracer ($SF_6$) Ages, and Water Vapor Isotope (D, T) Tracers, J. Atmos. Chem. 39, 303–325, 2001. 26201, 26208





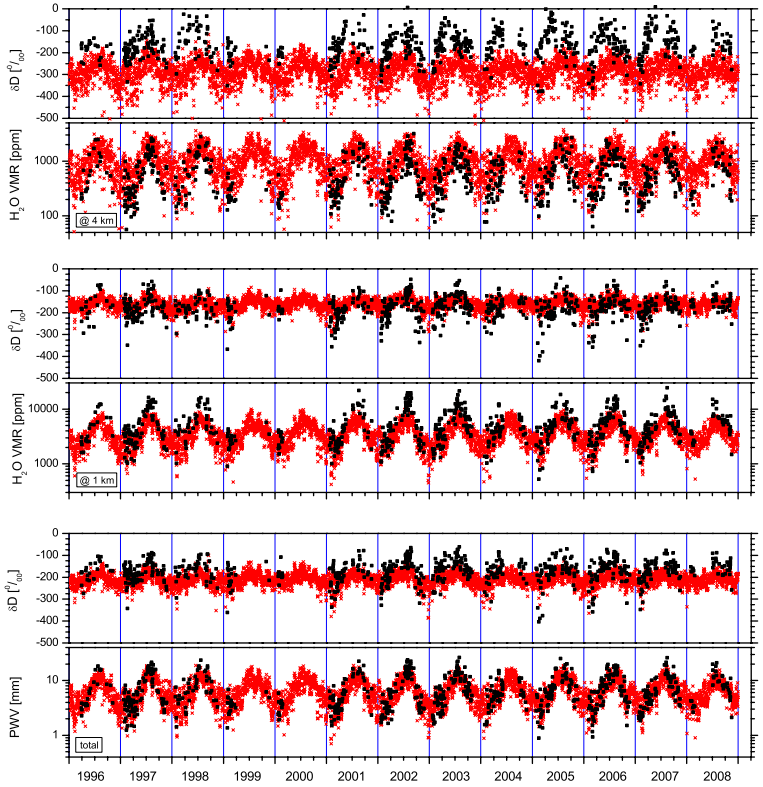


**Fig. 1.** Kiruna $H_2O$ and $\delta$D time series. Black squares: ground-based FTIR measurements; Red crosses: IsoGSM simulations; Panels from the bottom to the top: column integrated atmosphere, lower troposphere (altitude of 1 km), middle troposphere (altitude of 4 km).



ACPD
9, 26199–26235, 2009



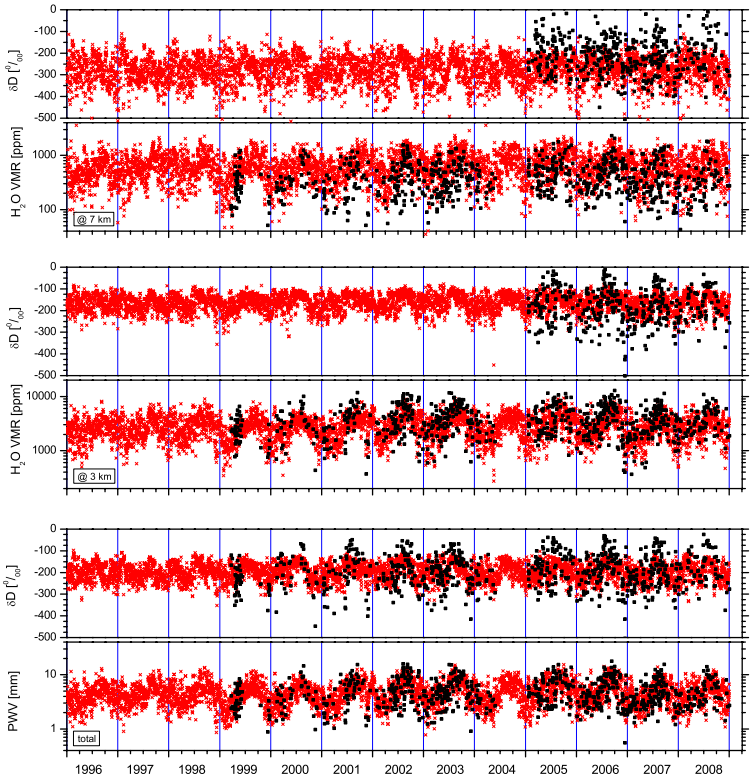


**Fig. 2.** Same as Fig. 1, but for Izaña. The altitudes representing the lower free troposphere and the middle troposphere are 3 and 7 km, respectively.



ACPD

9, 26199–26235, 2009



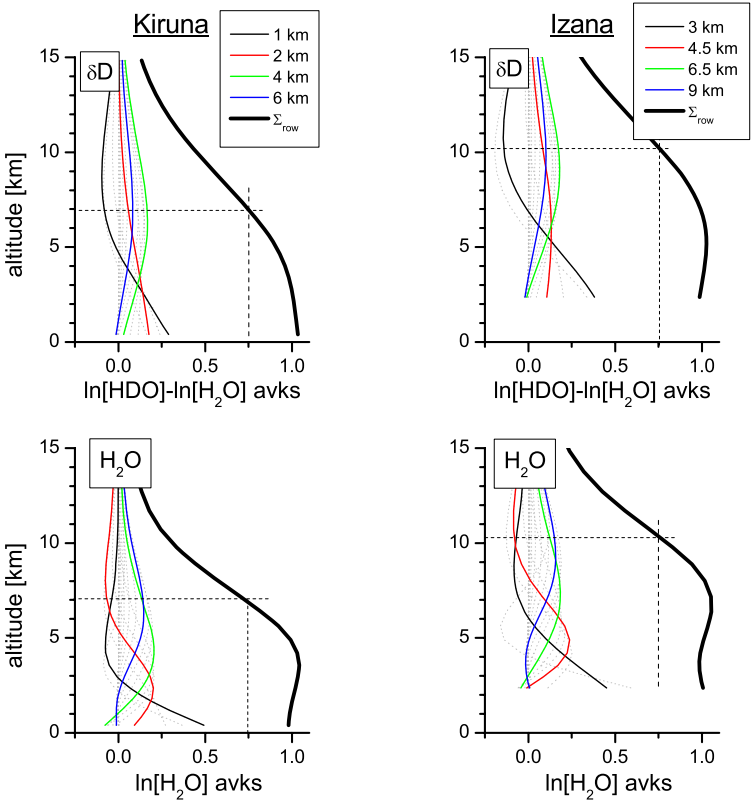


**Fig. 3.** FTIR Averaging kernels for $H_2O$ (bottom panels) and $\delta$D (expressed as $\ln[HDO] - \ln[H_2O]$, top panels). Left panels for Kiruna and right panels for Izaña.



ACPD
9, 26199–26235, 2009

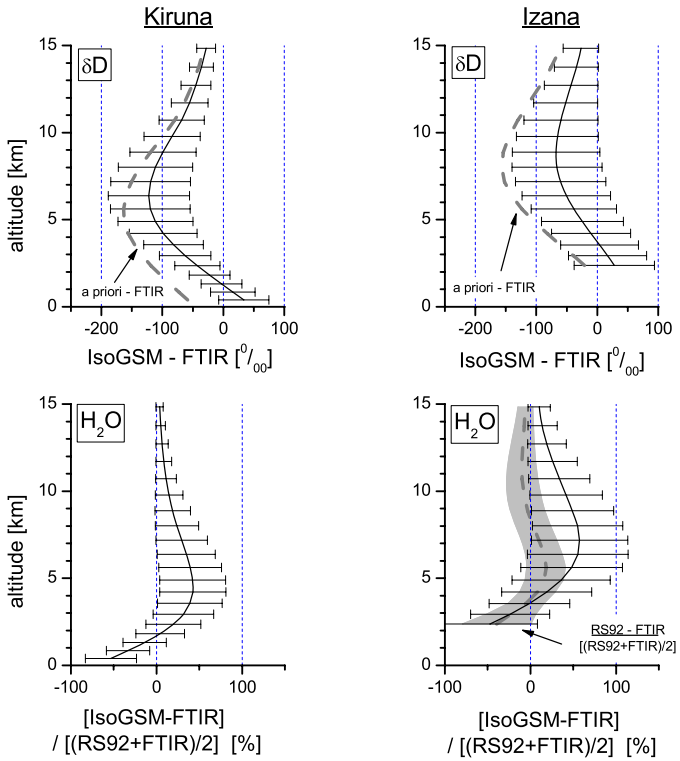


**Fig. 4.** Statistics for the difference between coincident FTIR profile measurements and IsoGSM profile simulations. Bottom panels: $H_2O$, top panels: $\delta$D. Left panels: Kiruna, right panels: Izaña. The grey area in the right bottom panel shows the comparison between Vaisala RS92 and FTIR measurements (grey dotted line: mean; grey area: 1$\sigma$ standard deviation). The grey dotted lines in the top panels show the difference between the mean retrieved FTIR $\delta$D values and the a priori $\delta$D profile, which has been constructed from in-situ $\delta$D measurements.



ACPD
9, 26199–26235, 2009

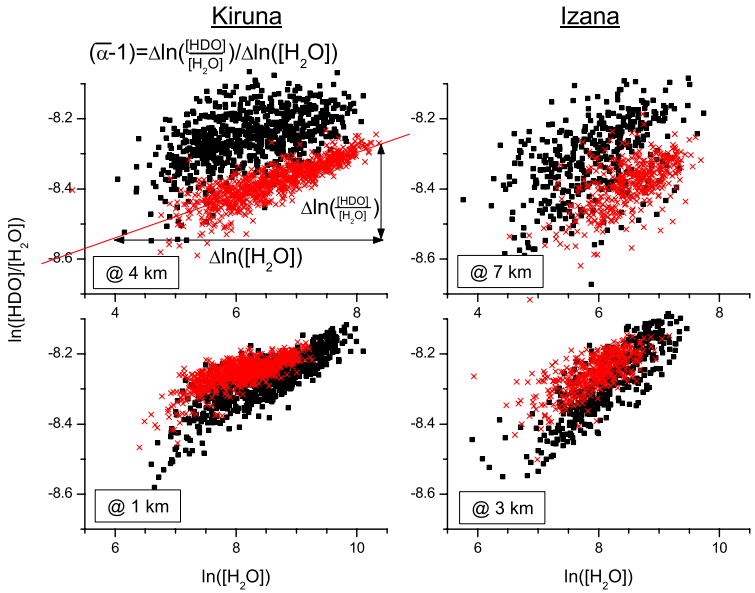


**Fig. 5.** Correlation between ln[$H_2O$] amounts and the $\delta$D values (expressed as ln$\frac{[HDO]}{[H_2O]}$), for the lower and middle troposphere (bottom and top panels, respectively). Left panel: for Kiruna; Right panel: for Izaña. Black solid squares represent FTIR measurements and red crosses IsoGSM simulations.



ACPD
9, 26199–26235, 2009

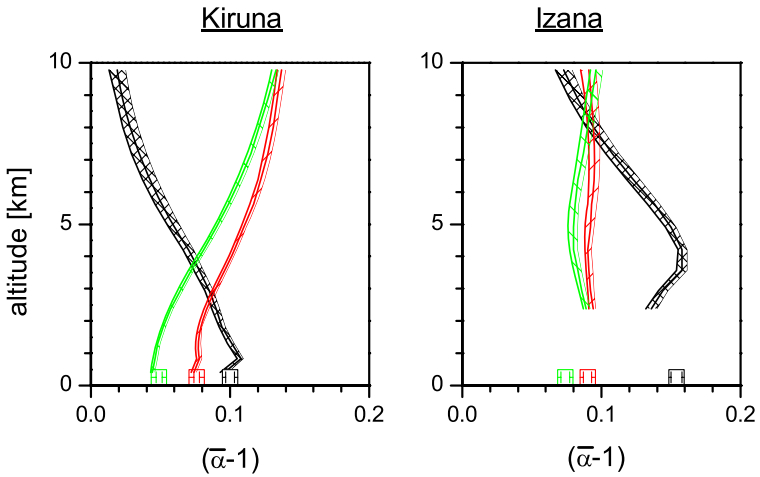


**Fig. 6.** Slope $(\overline{\alpha}-1)$ throughout the troposphere. Left panel for Kiruna and right panel for Izaña. Black, red, and green lines represent the FTIR measurements, the nudged model run, and the free model run, the hatched areas represent the $1\sigma$ significance intervals. The open squares upon the bottom x-axis represent the slope $(\overline{\alpha}-1)$ for the column integrated data.



ACPD
9, 26199–26235, 2009

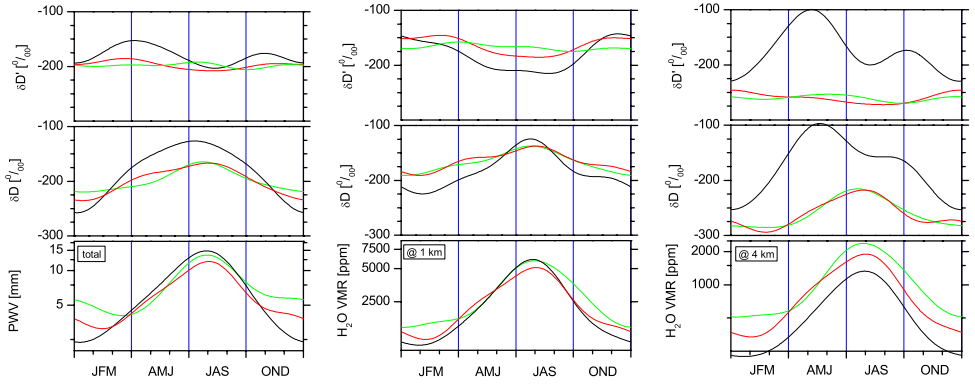


**Fig. 7.** Annual cycles for $H_2O$, $\delta$D, and $\delta$D' for Kiruna. Panels from the left to the right: column integrated atmosphere, lower free troposphere, and middle troposphere. Black line: FTIR, red line: nudged-run IsoGSM, green line: free-run IsoGSM.



ACPD
9, 26199–26235, 2009



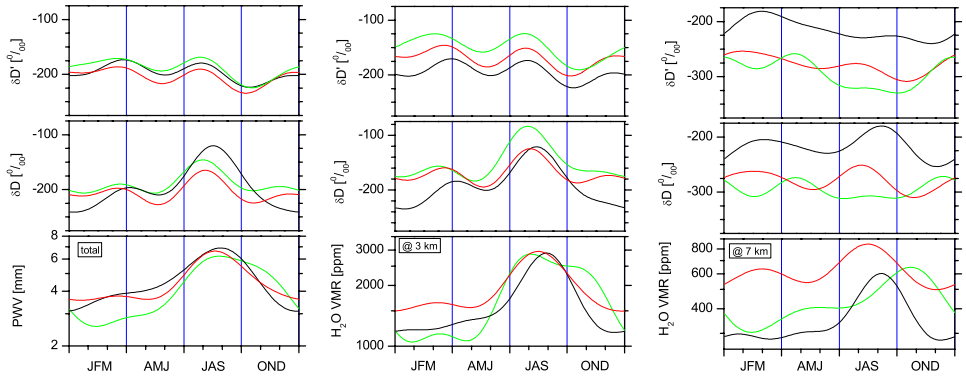


**Fig. 8.** Same as Fig. 7, but for the subtropical site of Izaña.



ACPD
9, 26199–26235, 2009



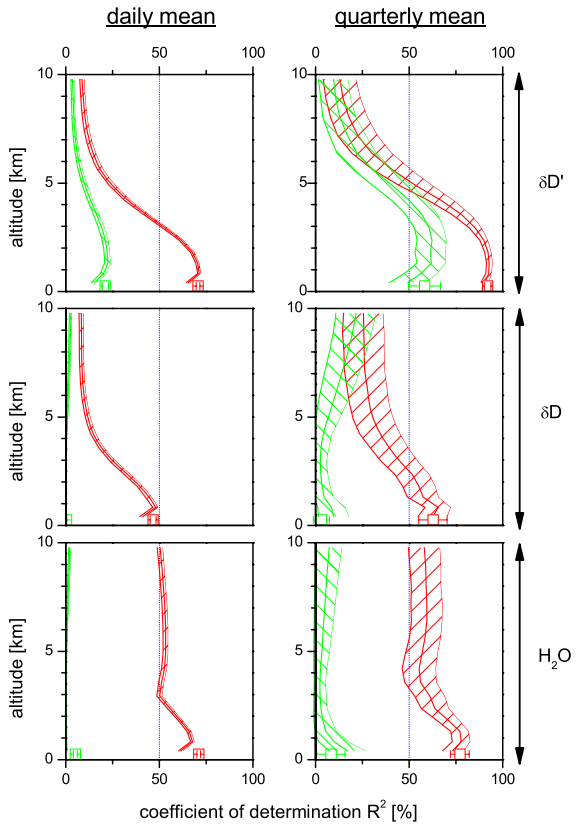


**Fig. 9.** Profiles of the coefficients of determination $R^2$ between deseasonalised FTIR and IsoGSM data of Kiruna. From the bottom to the top: $H_2O$ ($H_2O$ variability expressed as ln[$H_2O$]), $\delta$D, and $\delta$D' ($\delta$D and $\delta$D' variability expressed as $\ln \frac{[HDO]}{[H_2O]}$). Left: daily mean data, right: quarterly mean data. Red curve for nudged and green curve for free run IsoGSM (hatched area represents the 1$\sigma$ significance intervals).



ACPD
9, 26199–26235, 2009



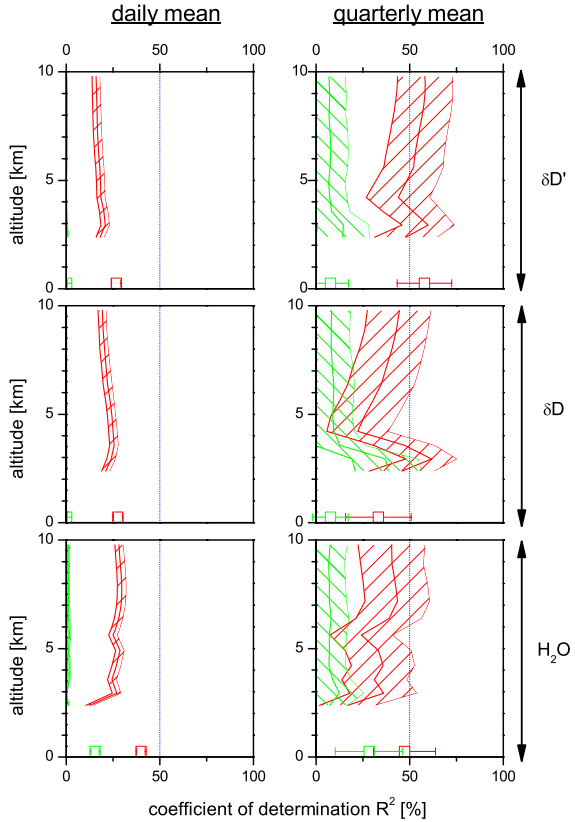


**Fig. 10.** Same as Fig. 9 but for Izaña.



ACPD
9, 26199–26235, 2009

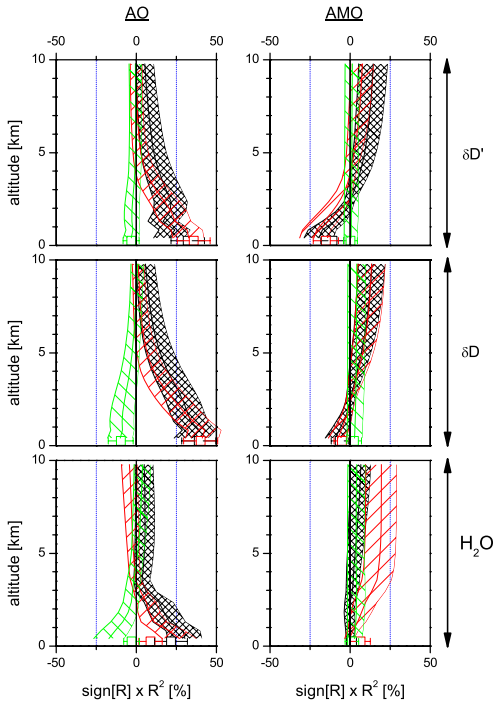


**Fig. 11.** Influence of the AO and the AMO on Kiruna's troposphere: vertical profiles of the coefficients of determination $R^2$ between quarterly mean FTIR and IsoGSM data, on the one hand, and the AO and AMO Index, on the other hand. Left panels: correlation with AO Index; right panels: correlations with AMO Index; panels from bottom to top: correlations with $H_2O$ ($H_2O$ anomaly expressed as $\ln[H_2O]$), with $\delta$D, and with $\delta$D' ($\delta$D and $\delta$D' anomaly expressed as $\ln\frac{[HDO]}{[H_2O]}$). Black line: FTIR data; red line: nudged-run IsoGSM data; green line: free-run IsoGSM data. The hatched areas represent the 1$\sigma$ significance intervals.



ACPD
9, 26199–26235, 2009



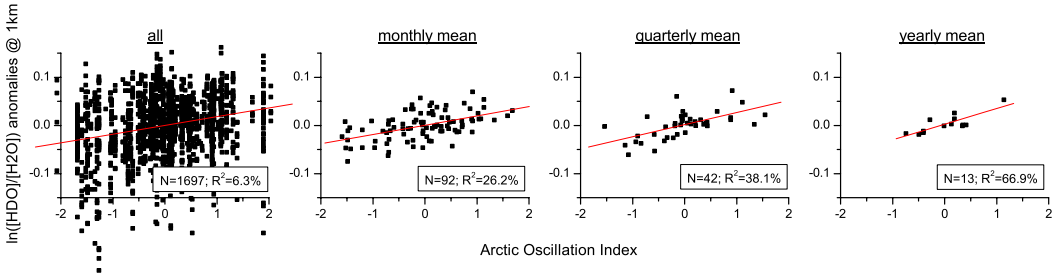


**Fig. 12.** Correlation plots between AO and $\delta$D anomalies (expressed as $\ln\frac{[HDO]}{[H_2O]}$) at an altitude of 1 km at Kiruna. From the left to the right: all individual measurements, monthly mean data, quarterly mean data, yearly mean data. The respective number of data points ($N$) and coefficients of determination ($R^2$) are written in each panel.



ACPD
9, 26199–26235, 2009



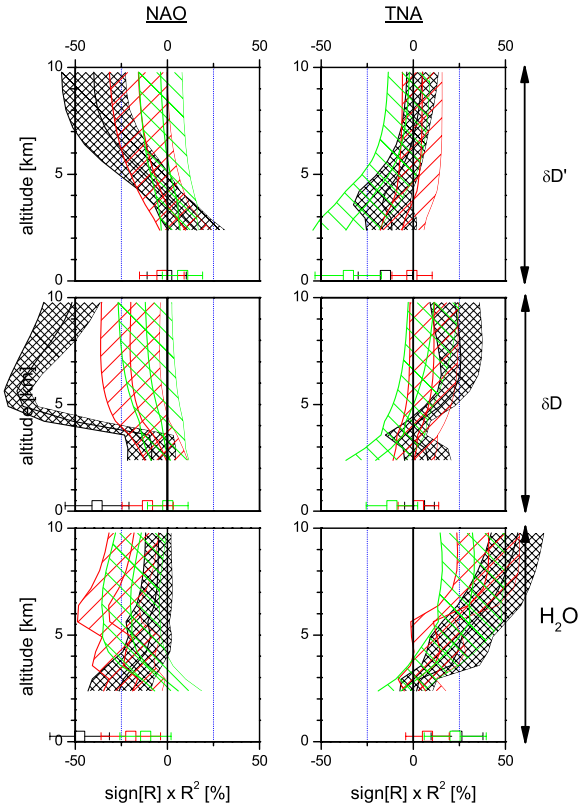


**Fig. 13.** Same as Fig. 11 but for Izaña and for correlations with NAO and TNA.



ACPD
9, 26199–26235, 2009